Wave-Function Hybridization in Yu-Shiba-Rusinov Dimers

Michael Ruby,[1] Benjamin W. Heinrich,[1] Yang Peng,[2,3,4] Felix von Oppen,[2] and Katharina J. Franke[1]
[1]Fachbereich Physik, Freie Universität Berlin, 14195 Berlin, Germany
[2]Dahlem Center for Complex Quantum Systems and Fachbereich Physik, Freie Universität Berlin, 14195 Berlin, Germany
[3]Institute of Quantum Information and Matter and Department of Physics, California Institute of Technology, Pasadena, California 91125, USA
[4]Walter Burke Institute for Theoretical Physics, California Institute of Technology, Pasadena, California 91125, USA

(Received 2 January 2018; published 11 April 2018)

Magnetic adsorbates on superconductors induce local bound states within the superconducting gap. These Yu-Shiba-Rusinov (YSR) states decay slowly away from the impurity compared to atomic orbitals, even in 3D bulk crystals. Here, we use scanning tunneling spectroscopy to investigate their hybridization between two nearby magnetic Mn adatoms on a superconducting Pb(001) surface. We observe that the hybridization leads to the formation of symmetric and antisymmetric combinations of YSR states. We investigate how the structure of the dimer wave functions and the energy splitting depend on the shape of the underlying monomer orbitals and the orientation of the dimer with respect to the Pb lattice.

DOI: 10.1103/PhysRevLett.120.156803

Magnetic adatoms on superconductors induce a local pair-breaking potential which binds Yu-Shiba-Rusinov (YSR) states inside the superconducting energy gap [1–3]. The symmetry of the potential derives from the orbital symmetry of the spin-polarized states of the adsorbate [4–6]. If the substrate imposes a sufficiently strong crystal field, the degeneracy of the adatom d levels, and consequently also of the YSR states, will be lifted [6,7]. It was already predicted by Rusinov that the YSR wave functions of two nearby adatoms hybridize and form bonding and antibonding combinations when the magnetic moments of the adatoms align ferromagnetically [3]. Subsequent theoretical studies explored the spatial structure of the YSR patterns [8,9] and the phase diagram [10] for YSR dimers. Many theoretical treatments assumed classical adatom spins with fixed alignment. Additional energy scales such as Hund couplings, crystal fields, and magnetocrystalline anisotropies affect the interaction of the magnetic adatoms [11,12]. In quantum spin systems, Kondo screening also needs to be considered [12–14].

YSR states have considerable lateral extent away from the magnetic adatom [15,16]. This leads to wave-function hybridization and energy splitting of YSR states in dimers of magnetic adatoms. Recent experimental studies observed these splittings for manganese (Mn) atoms on Pb(111), cobalt-phthalocyanine on $NbSe_2$, and chromium on β-Bi_2Pd [17–19]. While the latter two systems exhibit only a single YSR resonance, Mn adatoms on Pb(111) show several crystal-field-split YSR states [6]. Starting with Ref. [17], the earlier experiments already provided some indications of bonding and antibonding YSR states, but did not resolve how different YSR states are affected by the coupling to a neighboring adatom and how the orbital nature of the YSR states influences their hybridization.

Here, we present a scanning tunneling microscopy and spectroscopy (STM/STS) study of dimers of Mn adatoms on Pb(001). The Mn adatoms adsorb in hollow sites with a square-pyramidal crystal field that governs the orbital wave functions of the YSR states. We resolve symmetric and antisymmetric combinations of the individual YSR wave functions as well as a distinct distance and angle dependence of the hybridization of the YSR states. Our experimental study is complemented by a theoretical analysis of YSR dimers that takes the orbital structure of the impurity states into account.

We used a SPECS JT-STM under UHV conditions at a base temperature of 1.2 K. The Pb(001) single crystal ($T_c = 7.2$ K) was cleaned by cycles of Ne^+ sputtering and annealing. Mn adatoms were evaporated onto the cold sample in the STM ($T < 10$ K). We only analyzed pairs of adatoms that retain a distance ≥ 2.3 nm to other impurities. Within our resolution, this ensures the absence of any influence of other adatoms on the YSR states of the dimers. Energy resolution beyond the Fermi-Dirac limit is achieved by covering the W tips with a layer of Pb until the tip shows bulklike superconductivity [20]. This allows us to reach an effective energy resolution of ≈ 80 μeV. In first approximation, measurements with a superconducting tip probe a convolution of tip and sample density of states, which shifts all spectral features by the tip's gap parameter $\pm\Delta_{\mathrm{tip}}/e$.

We begin by reviewing the YSR states of isolated Mn adatoms on Pb(001) [Fig. 1(a)] [6]. Differential conductance spectra acquired with a superconducting tip show two pairs of Bardeen-Cooper-Schrieffer (BCS) singularities near a sample bias of ± 2.65 mV [20]. For a single Mn adatom, we find three additional pairs of YSR resonances inside the superconducting gap [Fig. 1(a)]. Assuming that

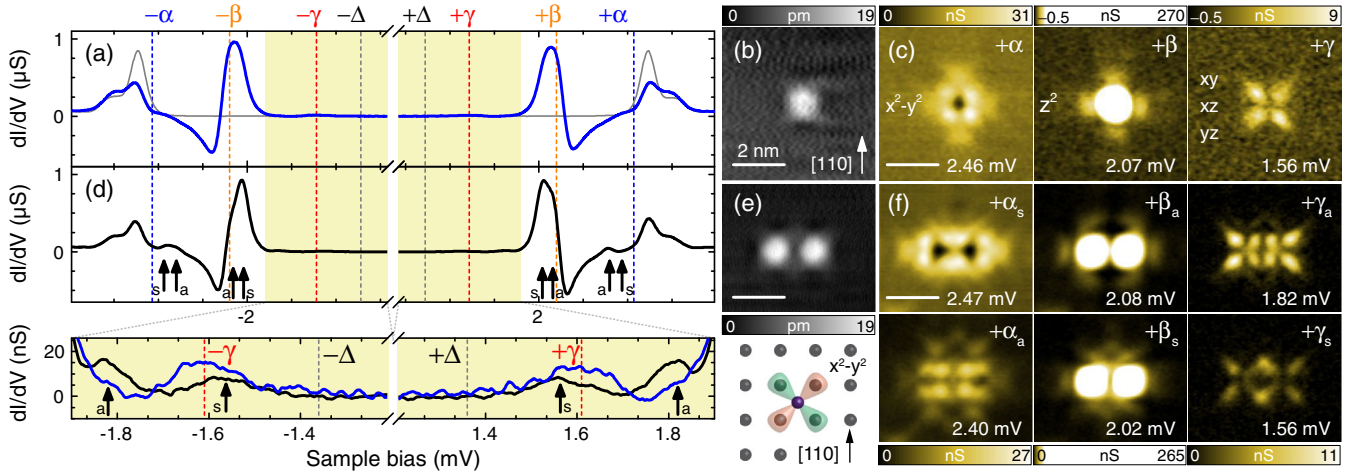

FIG. 1. (a) dI/dV spectrum at the center of the single Mn adatom shown in (b). Three subgap resonances ($\pm\alpha$, $\pm\beta$, $\pm\gamma$) and the tip gap ($\pm\Delta$) are marked in the spectrum by dashed vertical lines (blue, orange, red, gray). For reference, a trace taken on the pristine substrate is superimposed (solid gray line). Set point: 300 pA, 5 mV. (c) dI/dV maps of a monomer at $+\alpha$, $+\beta$, and $+\gamma$, covering the same area as in (b). (d) dI/dV spectrum of the dimer shown in (e), which is oriented along the $[1\bar{1}0]$ direction and separated by 1.38 ± 0.08 nm. Each subgap state is split into two resonances $\alpha_{s,a}$, $\beta_{s,a}$, and $\gamma_{s,a}$ (marked by arrows). Set point: 200 pA, 4 mV. Lock-in: 912 Hz, 15 μV_{rms}. (f) dI/dV maps taken at the positive-energy YSR resonances as marked in the figure. The scale for the resonances β in (c) and for $\beta_{a,b}$ in (f) is cut to emphasize the laterally extended intensity around the high intensity at the impurity center.

the Mn adatom is in a d^5 configuration, it conserves the orbital angular momentum of electrons in the superconductor and binds them in the d channel [4,6]. The hollow adsorption site imposes a square pyramidal crystal field, which lifts the degeneracy of the d states. Simple considerations of crystal field theory can be applied to deduce the order of the energy levels. The $d_{x^2-y^2}$ state lies highest in energy, followed by the d_{z^2} orbital at an intermediate and the degenerate d_{xy}, d_{xz}, d_{yz} states at the lowest energy. This explains the characteristic shapes of the YSR states in the dI/dV maps [Fig. 1(c)] [6]. Moreover, the observation of distinct d-orbital-like bound-state patterns implies that Hund's energy is larger than the energy splitting of the adatom d levels. The most intense resonance labeled by β arises from the d_{z^2} state. The faint resonance close to the superconducting gap edge (labeled α) derives from the $d_{x^2-y^2}$ state, and the lowest lying resonance (labeled γ) is a mixture of scattering at the degenerate d_{xy}, d_{xz}, and d_{yz} states. Tunneling into the d_{xy} state is less favorable than into the d_{xz}, and d_{yz} states, so that the dI/dV maps are dominated by the shapes of the d_{xz}- and d_{yz}-like orbitals [6].

Now consider a dimer of Mn adatoms oriented along the $[1\bar{1}0]$ direction [topography in Fig. 1(e)]. The Mn-Mn distance of 1.38 ± 0.08 nm corresponds to a separation of four lattice spacings (i.e., the distance between nearest-neighbor adsorption sites along $\langle 110 \rangle$). dI/dV spectra on the adatoms of the dimer reveal that each single-atom YSR resonance splits into two [Fig. 1(d)]. Moreover, dI/dV maps at the energies of the YSR resonances again exhibit characteristic shapes [Fig. 1(f)]. Many features of the maps for individual atoms can be recognized. For instance, the clover shapes of the $d_{x^2-y^2}$ and of the d_{xz}, d_{yz} states are still seen in the split α and γ states, respectively. The strong intensity of the d_{z^2}-derived YSR resonance β is also found on the dimer constituents.

However, a more detailed inspection reveals distinct differences between the maps for monomers and dimers. This is most clearly observed for the split γ resonance. The resonance $+\gamma_s$ exhibits two pairs of overlapping lobes in between the adatoms which are increased in intensity compared to the outer lobes. In contrast, $+\gamma_a$ has outer lobes of increased intensity, while the inner lobes have reduced intensity and do not overlap. There is a nodal line perpendicular to the dimer axis. Similar behavior is also observed for α, where the overall intensity is shifted outwards for α_a, but inwards for α_s. Only minor variations are observed for β, yet with a similar trend and a nodal line in the case of β_a. We interpret these modified intensity distributions as fingerprints of symmetric (s) and antisymmetric (a) combinations of YSR wave functions, hence the indices used above. For sketches of the d orbitals giving rise to the hybridized YSR states, see Fig. S1 in the Supplemental Material [21]. Interestingly, while the antisymmetric $+\gamma_a$ and $+\beta_a$ resonances have higher energy than $+\gamma_s$ and $+\beta_s$, respectively, it is the symmetric state that is higher in energy in the case of $+\alpha$. The relatively small energy splittings and the preservation of the characteristic orbital shapes indicate a small hybridization strength which does not lead to a change in the order or a mixture of YSR states derived from the individual adatoms.

These observations suggest that to a good approximation, we can describe the coupled YSR states as linear combinations of individual YSR wave functions. Moreover, a

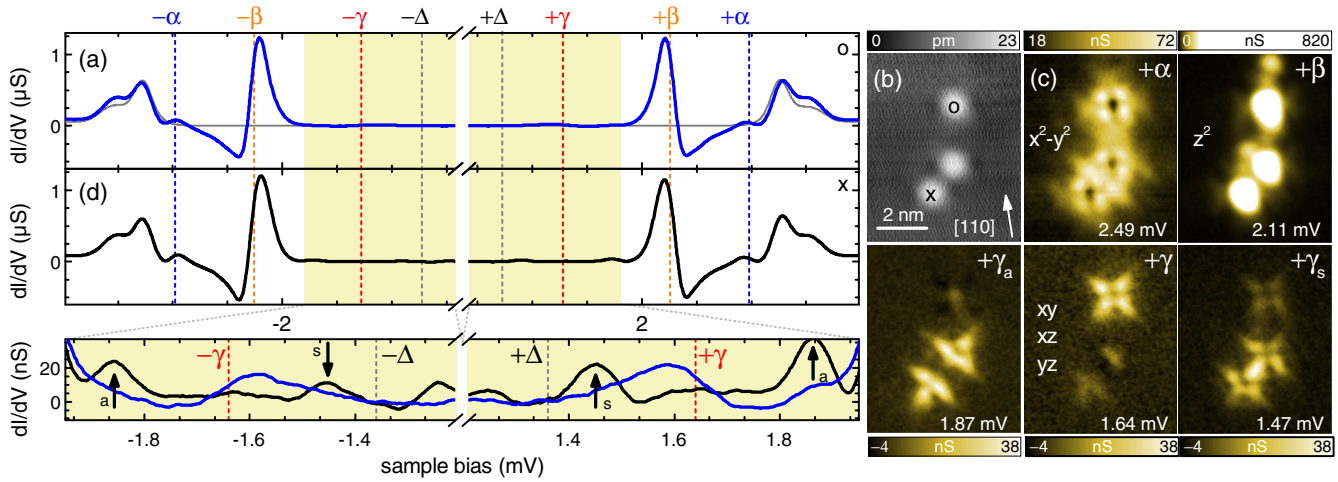

FIG. 2. (a) dI/dV spectrum at the center of the single Mn. Three subgap resonances ($\pm\alpha$, $\pm\beta$, $\pm\gamma$) and the tip gap ($\pm\Delta$) are marked in the spectrum by dashed vertical lines (blue, orange, red, gray). For reference, a trace taken on the pristine substrate is superimposed (solid gray line). Set point: 300 pA, 5 mV. Lock-in: 912 Hz, 15 μV_{rms}. (b) Topography and (c) dI/dV maps of three Mn adatoms, two of which form a dimer oriented along the [100] direction and separated by 1.47 ± 0.08 nm. (d) dI/dV spectrum of the dimer shown in (b). γ is split into two resonances $\gamma_{s,a}$ (marked by arrows). A faint signal at the energy of the monomer $\pm\gamma$ peaks hints at a third resonance. Set point: 200 pA, 4 mV.

splitting of YSR states can only occur if their spin wave functions are not orthogonal [22,23]. This implies that the alignment of the adatom spins is not antiferromagnetic, consistent with theoretical expectations [22]. The energy of the molecular YSR states can be obtained by analogy to the linear combination of atomic orbitals in a H_2 molecule (for details, see Supplemental Material [21]). This yields $E_\pm = E_s + (C \pm D/1 + S)$ for the energies of the YSR states. Here, E_s denotes the energy of the single impurity, $C_{ij} = \int d\boldsymbol{r} J(\boldsymbol{r} + d\hat{\mathbf{y}}) \phi_i^\dagger(\boldsymbol{r}) \phi_j(\boldsymbol{r})$ a Coulomb-like integral, $D_{ij} = \int d\boldsymbol{r} J(\boldsymbol{r}) \phi_i(\boldsymbol{r})^\dagger \phi_j(\boldsymbol{r} + d\hat{\mathbf{y}})$ an exchangelike integral, and $S_{ij} = \int d\boldsymbol{r} \phi_i(\boldsymbol{r})^\dagger \phi_j(\boldsymbol{r} + d\hat{\mathbf{y}})$ an overlap integral with $\phi_{i,j}$ being the YSR wave function deriving from one of the five d orbitals. We notice that the Coulomb-like integral C provides a shift and the exchangelike integral D produces a splitting. C falls off monotonically with distance $d\hat{\mathbf{y}}$ (choosing the dimer axis along the y direction) and has the same sign as $J(\boldsymbol{r})$. It is thus positive or negative depending on whether the coupling between the impurity and the itinerant electrons is antiferromagnetic or ferromagnetic. The sign of the exchangelike integral D alternates as a function of separation d because the YSR wave function $\phi(\boldsymbol{r})$ oscillates with the Fermi wavelength λ_F. Hence, unlike the case of atomic orbitals in H_2, the order in energy does not reflect whether the wave function is symmetric or antisymmetric. In view of our experimental results, this explains why $+\gamma_a$ and $+\beta_a$ have a larger energy than $+\gamma_s$ and $+\beta_s$, respectively, whereas the order of symmetric and antisymmetric YSR wave functions is reversed in the case of α with $+\alpha_s$ having larger energy than $+\alpha_a$. One should therefore avoid calling these states bonding or antibonding.

To further validate these interpretations, we also investigated Mn dimers oriented along the $\langle 100 \rangle$ directions of the Pb lattice. Figure 2 shows experimental results for such a dimer with a separation of 1.47 ± 0.08 nm or three lattice spacings along $\langle 100 \rangle$. The dI/dV spectrum in Fig. 2(d) shows no splitting for the α and β resonances, and the corresponding dI/dV maps in Fig. 2(c) resemble simple superpositions of the single-adatom maps. (Note also that the third adatom in the vicinity exhibits the spectrum of an isolated Mn adatom.) The γ resonance shows a sizable splitting into two and hints of an additional resonance. The latter remains at the original position of the γ resonance of the monomer. The absence of a shift or splitting suggests that its hybridization is negligible. The smallest overlap is expected for the d_{xz}-like YSR states. The dI/dV map of the unshifted resonance shows faint intensity consistent with the shape of the d_{xz}-like YSR state [Fig. 2(c) bottom, middle]. The split-off γ resonances would then originate from linear combinations of the d_{yz}- and d_{xy}-like YSR states which have hybridizations of (nearly) equal strength. A symmetric combination of the d_{yz}-like monomer states is reflected in the strong intensity along the bonding direction at the resonance energy deeper inside the superconducting gap (γ_s). The dI/dV map of the resonance closer to the gap edge (γ_a) shows no intensity along the bonding direction. It thus indicates the antisymmetric combination of monomer states. The dI/dV maps at both γ_s and γ_a exhibit intensity perpendicular to the bonding direction. This would then originate from the d_{xy}-like YSR states, possibly distorted by the Pb atom lying on the dimer axis. This interpretation is in agreement with theoretical symmetry considerations (see discussion and Fig. S2 in the Supplemental Material [21]).

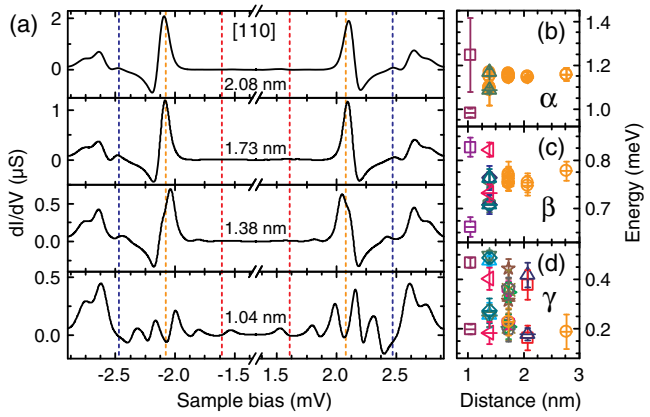

FIG. 3. (a) dI/dV spectra of Mn dimers with different interatomic distances oriented along the ⟨110⟩ direction. Spectra are recorded at the center of one of the adatoms of a pair. Setpoint: 200 pA, 4 mV. (b)–(d) The splitting in energy of the peaks α, β, and γ as a function of the interatomic distance for the ⟨110⟩ direction. The same color and symbol indicate split pairs of resonances from the same dimer spectrum. Different symbols and colors correspond to data from different dimers except for yellow circles, which indicate data points where no splitting was observed for the respective resonance.

Figures 3 and 4 collect experimental results for the separation dependence of the resonance splittings. Figure 3 focuses on dimers oriented along ⟨110⟩. Panel (a) shows four spectra for separations of three to six lattice spacings. Panels (b)–(d) collect the YSR resonance energies for additional dimers. For adatom separations of $d = 2.77$ nm (eight lattice spacings), none of the YSR resonances is split within our energy resolution of ≈ 80 μeV. The splitting of the $d_{x^2-y^2}$-derived YSR resonance α is resolved for one (out of four) of the observed dimers with a separation of 1.38 nm (four lattice spacings). For smaller adatom distances, we resolve the splitting in all dimers, with splittings of ≈ 0.2 meV for $d = 1.04$ nm (three lattice spacings). The splitting of the d_{z^2}-derived YSR resonance sets in at the same separation and is of approximately the same magnitude. In comparison, the d_{xy}, d_{xz}, d_{yz}-derived YSR resonance γ already splits at larger distances ($d < 2.08$ nm), with splittings up to ≈ 0.3 meV for the smallest dimers.

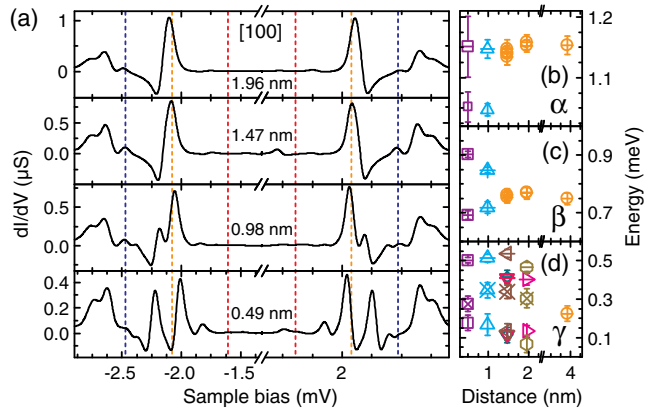

FIG. 4. (a) dI/dV spectra of Mn dimers with different interatomic distances oriented along the ⟨100⟩ direction. Spectra are recorded at the center of one of the adatoms of a pair. Set point: 200 pA, 4 mV. (b)–(d) The splitting in energy of the peaks α, β, and γ as a function of the interatomic distance for this orientation. Same color code as in Fig. 3 (b)–(d).

The splittings of the YSR resonances in dimers oriented along ⟨100⟩ show similar behavior. Figure 4 shows four representative spectra as well as the extracted energy positions of the YSR resonances. The splitting of the $d_{x^2-y^2}$- and the d_{z^2}-derived YSR resonance is only observable for $d \leq 0.98$ nm (two lattice spacings) with a splitting of ≈ 0.1 and ≈ 0.2 meV, respectively, at $d = 0.49$ nm (one lattice spacing). The extracted $d_{x^2-y^2}$-derived resonances hint at an overall downward shift with decreasing distance. As already described above, we observe a splitting of the γ resonance into three components for many (though not all) dimers with the central resonance remaining at the energy of the monomer (see the discussion of the faint resonances at $\pm\gamma$ seen in Fig. 2).

In addition to the decay with adatom separation, theory predicts an oscillatory behavior of the energy splitting with a period of half the Fermi wavelength λ_F (see discussion above and Supplemental Material [21]). For Pb, $\lambda_F/2$ of the outer Fermi sheet, which gives rise to the YSR states [6], equals 0.61 ± 0.03 nm along the ⟨110⟩ direction and 0.53 ± 0.06 nm along the ⟨100⟩ direction [24]. The range over which we resolve the energy splitting is only slightly larger than $\lambda_F/2$ and contains only three distinct separations due to the discreteness of the adsorption sites. This precludes testing the oscillatory behavior of the YSR splitting in our experiments. Moreover, we may only extract a hint of a distance-dependent shift of the center of mass of the YSR resonances for the γ resonances of the ⟨110⟩ dimers. Depending on the particular resonance, theory predicts a shift of at most one quarter of the energy splitting (see Supplemental Material [21]), which is at the limit of our energy resolution.

In conclusion, we resolved and analyzed the hybridization of YSR states originating from Mn adatoms which are located three to six lattice spacings apart on Pb(001) and observe characteristic energy splittings of up to a few hundred μeV. At these relatively large distances, direct exchange coupling or simple superexchange via a single substrate atom can be neglected. Instead, we show by mapping the spatial distribution of the dimer YSR states that the coupling hybridizes monomer YSR states into symmetric and antisymmetric linear combinations. The observed hybridization precludes antiferromagnetic alignment of the adatom magnetic moments. We have also recorded dI/dV spectra with a spin-polarized tip, but did not observe any spin contrast with oppositely magnetized tips or varying contrast in different dimers.

This suggests that the spin orientation fluctuates due to thermal excitations.

The hybridization strength is comparable to the RKKY coupling on normal metal surfaces [25]. When coupling adatoms in an entire chain, one expects the formation of YSR bands. These may give rise to topological superconductivity and an alternative route towards the realization of Majorana bound states [26–28]. To date, adatom-based Majorana experiments rely on compact ferromagnetic chains, in which the direct coupling of adatom d states is presumably essential for the formation of a topological superconducting phase [29–34].

We gratefully acknowledge funding by the Deutsche Forschungsgemeinschaft through HE7368/2, FR2726/4, and CRC 183, as well as the ERC consolidator grant NanoSpin.

[1] L. Yu, Acta Phys. Sin. **21**, 75 (1965).
[2] H. Shiba, Prog. Theor. Phys. **40**, 435 (1968).
[3] A. I. Rusinov, Zh. Eksp. Teor. Fiz. Pisma Red. **9**, 146 (1968) [JETP Lett. **9**, 85 (1969)].
[4] J. R. Schrieffer, J. Appl. Phys. **38**, 1143 (1967).
[5] C. P. Moca, E. Demler, B. Jankó, and G. Zaránd, Phys. Rev. B **77**, 174516 (2008).
[6] M. Ruby, Y. Peng, F. von Oppen, B. W. Heinrich, and K. J. Franke, Phys. Rev. Lett. **117**, 186801 (2016).
[7] D.-J. Choi, C. Rubio-Verdú, J. de Bruijckere, M. M. Ugeda, N. Lorente, and J. I. Pascual, Nat. Commun. **8**, 15175 (2017).
[8] M. E. Flatté and D. E. Reynolds, Phys. Rev. B **61**, 14810 (2000).
[9] D. K. Morr and N. A. Stavropoulos, Phys. Rev. B **67**, 020502 (2003).
[10] N. Y. Yao, C. P. Moca, I. Weymann, J. D. Sau, M. D. Lukin, E. A. Demler, and G. Zaránd, Phys. Rev. B **90**, 241108 (2014).
[11] R. žitko, O. Bodensiek, and T. Pruschke, Phys. Rev. B **83**, 054512 (2011).
[12] N. Hatter, B. W. Heinrich, M. Ruby, J. I. Pascual, and K. J. Franke, Nat. Commun. **6**, 8988 (2015).
[13] K. J. Franke, G. Schulze, and J. I. Pascual, Science **332**, 940 (2011).
[14] K. Grove-Rasmussen, G. Steffensen, A. Jellinggaard, M. H. Madsen, R. žitko, J. Paaske, and J. Nygård, arXiv: 1711.06081.
[15] A. Yazdani, B. A. Jones, C. P. Lutz, M. F. Crommie, and D. M. Eigler, Science **275**, 1767 (1997).
[16] G. C. Ménard, S. Guissart, C. Brun, S. Pons, V. S. Stolyarov, F. Debontridder, M. V. Leclerc, E. Janod, L. Cario, D. Roditchev, P. Simon, and T. Cren, Nat. Phys. **11**, 1013 (2015).
[17] S.-H. Ji, T. Zhang, Y.-S. Fu, X. Chen, X.-C. Ma, J. Li, W.-H. Duan, J.-F. Jia, and Q.-K. Xue, Phys. Rev. Lett. **100**, 226801 (2008).
[18] S. Kezilebieke, M. Dvorak, T. Ojanen, and P. Liljeroth, arXiv:1701.03288 [Nano Lett. (to be published)].
[19] D.-J. Choi, C. G. Fernández, E. Herrera, C. Rubio-Verdú, M. M. Ugeda, I. Guillamón, H. Suderow, J. I. Pascual, and N. Lorente, arXiv:1709.09224.
[20] M. Ruby, B. W. Heinrich, J. I. Pascual, and K. J. Franke, Phys. Rev. Lett. **114**, 157001 (2015).
[21] See Supplemental Material at http://link.aps.org/supplemental/10.1103/PhysRevLett.120.156803 for a description of the theoretical analysis of orbital-dependent Yu-Shiba-Rusinov states and their hybridization in dimers, and numerical results thereof.
[22] N. Y. Yao, L. I. Glazman, E. A. Demler, M. D. Lukin, and J. D. Sau, Phys. Rev. Lett. **113**, 087202 (2014).
[23] S. Hoffman, J. Klinovaja, T. Meng, and D. Loss, Phys. Rev. B **92**, 125422 (2015).
[24] G. I. Lykken, A. L. Geiger, K. S. Dy, and E. N. Mitchell, Phys. Rev. B **4**, 1523 (1971).
[25] L. Zhou, J. Wiebe, S. Lounis, E. Vedmedenko, F. Meier, S. Blügel, P. H. Dederichs, and R. Wiesendanger, Nat. Phys. **6**, 187 (2010).
[26] S. Nadj-Perge, I. K. Drozdov, B. A. Bernevig, and A. Yazdani, Phys. Rev. B **88**, 020407(R) (2013).
[27] F. Pientka, L. I. Glazman, and F. von Oppen, Phys. Rev. B **88**, 155420 (2013).
[28] M. Schecter, K. Flensberg, M. H. Christensen, B. M. Andersen, and J. Paaske, Phys. Rev. B **93**, 140503(R) (2016).
[29] S. Nadj-Perge, I. K. Drozdov, J. Li, H. Chen, S. Jeon, J. Seo, A. H. MacDonald, B. A. Bernevig, and A. Yazdani, Science **346**, 602 (2014).
[30] M. Ruby, F. Pientka, Y. Peng, F. von Oppen, B. W. Heinrich, and K. J. Franke, Phys. Rev. Lett. **115**, 197204 (2015).
[31] R. Pawlak, M. Kisiel, J. Klinovaja, T. Meier, S. Kawai, T. Glatzel, D. Loss, and E. Meyer, Quantum Inf. Comput. **2**, 16035 (2016).
[32] B. E. Feldman, M. T. Randeria, J. Li, S. Jeon, Y. Xie, Z. Wang, I. K. Drozdov, B. A. Bernevig, and A. Yazdani, Nat. Phys. **13**, 286 (2017).
[33] M. Ruby, B. W. Heinrich, Y. Peng, F. von Oppen, and K. J. Franke, Nano Lett. **17**, 4473 (2017).
[34] S. Jeon, Y. Xie, J. Li, Z. Wang, B. A. Bernevig, and A. Yazdani, Science **358**, 772 (2017).